Accepted Manuscript

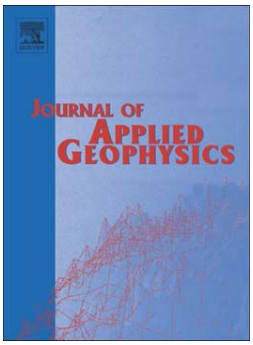

Time-lapse electrical resistivity imaging of the thermally affected zone of a Borehole Thermal Energy Storage system near Torino (Northern Italy)

N. Giordano, A. Arato, C. Comina, G. Mandrone

PII: S0926-9851(17)30305-1
DOI: doi:10.1016/j.jappgeo.2017.03.015
Reference: APPGEO 3247

To appear in: *Journal of Applied Geophysics*

Received date: 5 August 2016
Revised date: 10 March 2017
Accepted date: 28 March 2017

Please cite this article as: Giordano, N., Arato, A., Comina, C., Mandrone, G., Time-lapse electrical resistivity imaging of the thermally affected zone of a Borehole Thermal Energy Storage system near Torino (Northern Italy), *Journal of Applied Geophysics* (2017), doi:10.1016/j.jappgeo.2017.03.015

Time-lapse electrical resistivity imaging of the thermally affected zone of a Borehole Thermal Energy Storage system near Torino (Northern Italy).

N. Giordano[1], A. Arato[2], C. Comina[1], G. Mandrone[1]

[1] Dipartimento di Scienze della Terra - Università degli Studi di Torino, Via Valperga Caluso, 35 – 10125 Torino, Italy

[2] Techgea Srl – Loc. Amerique, 9 – 11020 Aosta, Italy (formerly at: DIATI - Politecnico di Torino, Corso Duca degli Abruzzi, 24 - 10129 Torino, Italy)

Abstract

A Borehole Thermal Energy Storage living lab was built up nearby Torino (Northern Italy). This living lab aims at testing the ability of the alluvial deposits of the north-western Po Plain to store the thermal energy collected by solar thermal panels and the efficiency of energy storage systems in this climatic context. Different monitoring approaches have been tested and analyzed since the start of the thermal injection in April 2014. Underground temperature monitoring is constantly undertaken by means of several temperature sensors located along the borehole heat exchangers and within the hydraulic circuit. Nevertheless, this can provide only pointwise information about underground temperature distribution. For this reason, a geophysical approach is proposed in order to image the thermally affected zone (TAZ) caused by the heat injection: surface electrical resistivity measurements were carried out with this purpose. In the present paper, results of time-lapse daily acquisitions are reported with the aim of imaging the thermal plume evolution within the subsoil. Resistivity data, calibrated on local temperature measurements, have shown their potentiality in imaging the heated plume of the system and depicting its evolution within the day. Different types of data processing were adopted in order to face issues mainly related to a highly urbanized environment. The use of apparent resistivity proved to be in valid agreement with the results of different inversion approaches. The inversion processes did not significantly improve the qualitative and quantitative TAZ imaging in comparison to the pseudo-sections. This suggested the usefulness of apparent resistivity data alone for a rough monitoring of TAZ in this kind of applications.

Keywords: electrical resistivity; thermally affected zone; borehole thermal energy storage.

Corresponding author:
Nicolò Giordano
nicolo.giordano@unito.it
Dipartimento di Scienze della Terra
Via Valperga Caluso, 35
10125 – TORINO
tel. +39 011 6705325

1. INTRODUCTION

Renewable energy sources, such as solar thermal energy, often suffer from the shortcoming that most of their supply takes place when the user demand is low (e.g. sun energy is mostly related to the warm season, when the heating demand is reduced). In this respect, several thermal energy storage techniques have been studied since the late 70s (Sharma et al., 2009; Xu et al., 2014, Cabeza, 2015). Underground thermal energy storage technologies have been developed to ensure reliability, efficiency and economic sustainability of the renewable heat. Given the development and the excellent performance of shallow Borehole Heat Exchangers (BHEs), some attempts have been successfully conducted by storing the heat within the subsoil in Borehole Thermal Energy Storage (BTES) systems (e.g. Bakema et al., 1995; Fisch et al., 1998; Reuss et al., 2006; Sibbit et al., 2012; Rapantova et al., 2016).

Both thermal and hydrogeological properties of the subsoil have to be carefully characterized for the design and operation of this kind of installations. Correct monitoring strategies also appear to be of major importance to better understand thermal exchange processes and environmental effects of low enthalpy geothermal applications and heat storage systems, particularly into highly populated areas. The Thermally Affected Zone (TAZ) generated within the storage volume should be considered and accurately imaged to assess the possible side adverse effects on the litho-, hydro- and bio-sphere. Typically, the TAZ is imaged through local and pointwise measurements by means of temperature sensors located within the system to monitor changes in underground temperatures. In this context, geophysics can be adopted to obtain complementary and spatially distributed information directly from the ground surface in a quick, cost-effective and non-invasive way.

Resistivity-based measurements are potentially very powerful since useful relationships can be found in literature between electrical resistivity, temperature and several relevant hydrogeological parameters. Underground resistivity is indeed related, even if in a complex way, to various soil and environmental attributes, such as total dissolved solids (TDS) in the fluid, mineral composition, porosity and water content (Friedman, 2005). Archie (1942) and Urish (1981), with theoretical and empirical results, were the first to demonstrate a correlation between the formation factor (the ratio between the bulk resistivity of the subsoil and the resistivity of interstitial fluid) of an aquifer and the pore water resistivity. This relation has then been widely adopted in characterization and monitoring studies. Resistivity surveys can therefore be useful to assess the properties of the shallow underground for the design of a low

enthalpy geothermal system. Moreover, given that electrical resistivity is strongly influenced by temperature (Rein et al., 2004; Hayashi, 2004; Hayley et al., 2007), promising applications of resistivity measurements can also take place in the monitoring phase. It is potentially possible to use resistivity variations as a recording factor in order to image time-lapse temperature distribution (e.g. Hermans et al., 2015; Arato et al., 2015) .

Easiness of operation and interpretation related to both hardware and software developments pushed the use of Electrical Resistivity Tomography (ERT) as one of the most used techniques in the field of characterization and monitoring of the subsurface. Surface ERT has many practical applications for studying soil properties and processes in the subsurface (e.g. Daily and Ramirez, 1992; LaBrecque et al., 1996b; Singh et al., 2001; Slater, 2007). Thereby, ERT represents a standard method for subsurface monitoring of different phenomena (see among others Ramirez et al., 1993; Zhou et al., 2001; Binley et al., 2002; Michot et al., 2003; Corwin and Lesch, 2005; Miller et al. 2008; Schwartz et al., 2008) and characterization of hydrogeological properties (Carrier, 2003; Slater, 2007) and parameters (Hoffman and Dietrich, 2004).

The use of ERT to exploit electrical resistivity as a key changing factor in temperature variation at both field and lab scale has been already conducted for different purposes: imaging of heated water injection (Benderitter and Tabbagh, 1982; Hermans et al., 2015), monitoring of gas-phase formation due to heat storage (Lüders et al., 2016), geothermal exploration (Bruno et al., 2000; Garg et al., 2007), monitoring the performance of low enthalpy ground source energy systems (Fragkogiannis et al., 2008; Firmbach et al., 2013) and localizing the burning front of underground coal fires (Revil et al., 2013) to name but a few. Nevertheless, more examples are particularly necessary in real scale applications, since calibrated, robust and reliable correlations between electric resistivity and temperature are not available yet (Robert et al., 2013). Indeed, several uncertainties stand at field scale where different factors do affect the underground resistivity distribution. Correct acquisition, elaboration and interpretation of resistivity surveys are challenging in highly populated areas where heat storage applications are usually designed. Particularly, artifacts related to the inversion problem can be critical for a correct imaging and quantification of thermally induced variations.

In this respect, the present paper aims to give an additional evaluation of the potential of ERT technique as a field-scale TAZ imaging tool. This work is a prosecution of laboratory

scale electrical measurements performed by Giordano et al. (2016b) and is based on time-lapse ERT surveys conducted at a BTES site. A field-scale BTES living lab was built up in Grugliasco, near the Topography Department of the University of Torino (Giordano et al., 2016a). The living lab has been working since April 2014. Underground temperature monitoring is constantly undertaken by means of several temperature sensors located along the BHEs and within the hydraulic circuit. Resistivity surveys were firstly performed monthly since the startup of the plant in order to image the evolution of the charge phase in the ground. However, too many factors, apart from temperature, can affect the resistivity distribution during a whole month. A single rainfall event can indeed completely reset the underground resistivity field, since the BHEs are drilled into unsaturated deposits. For this reason, time-lapse data presented in this paper were acquired during a single operation day during the charge phase. These data, calibrated on local temperature measurements, were used to image the TAZ of the system.

2. MATERIALS AND METHODS

2.1 Description of the BTES living lab

The test site where the BTES living lab has been constructed is located in the north-western portion of the Pianura Padana in the municipality of Grugliasco (Torino, Italy). The drilling activity performed in the area showed 30 m of Pleistocene-Holocene gravels and sands, sometimes with local decimetric layers of compacted gravelly sands. This unit overlies deposits of a transitional facies between marine and continental environment, being characterized by the alternation of coarse sands and silts due to the progression and regression of the coastal line in the Middle Pliocene – Lower Pleistocene (**Fig. 1**). On the strength of the available data, the water table of the unconfined aquifer is located at 35-40 m below ground level (b.g.l.) and the groundwater flows towards ESE. Groundwater flow has been demonstrated to improve the heat exchange between BHEs and the ground (Wang et al., 2009; Casasso and Sethi, 2014) thanks to its continuous supply of thermal energy. It conversely induces a significant decrease of the BTES efficiency since it can leach out the thermal energy stored into the aquifer and reducing the extracted/stored energy ratio (Nguyen et al., 2017).

Due to these geological conditions and owing to specific restrictions from the local authorities, the BTES plant was set up in the partially-saturated zone of the unconfined aquifer. This situation was however a valuable choice in order to test the ability of partially-

saturated alluvial deposits to store the heat. The underground part of the system stores the heat by means of four 27 m deep BHEs. The designed arrangement (**Fig. 1** and **2**) consists of a double U-pipe borehole (DU) placed in the center of an equilateral triangle (2 m side) and 3 single U-pipe BHEs (A, B and C) located at the vertexes of the triangle. The top of the BHEs is placed at a depth of 1.5 m b.g.l. in order to minimize heat losses towards the atmosphere. With this purpose, a layer of insulating filling material was added above the BHEs. A 33 m deep monitoring hole (MH) was located 2 m away from the double-U heat exchanger. The remaining part of the system is located in the nearby Topography Department (**Fig. 2**). Two solar thermal panels are placed on the roof and they collect solar energy with a total net surface of 5.0 m^2 and an inclination of approximately 10°. The circuit is governed by a hydraulic pump located in the basement of the building. The pump provides the heat transfer fluid (HTF) circulation through the whole system at a maximum flow rate of 210 l h^{-1} and a constant pressure of 2.2 bar.

The temperature monitoring system consists of 20 RTD 4wire Pt100 (measurement range -50 ÷ +180 °C, accuracy 5%) placed every 5 m down-hole in 3 of the 4 BHEs and in the monitoring hole. In addition, 10 temperature sensors of the same type are placed throughout the circuit and on the thermal panels. The operative mode of the system was decided according to similar operating plants, where a core volume benefits from the warmest carrier fluid and it is surrounded by an annular volume fed with the same fluid at a lower amount of heat. Therefore, during the "Charge Phase", the HTF warmed up by solar energy is driven down into the central BHE (DU), then out to the hydraulic pump and pumped again down into the outer BHEs (A, B and C). The system is able to evaluate whether to circulate the fluid or not according to a temperature difference constraint. If the difference between the collectors and the average ground temperature is more than 5°C, the system works and the ground is charged by solar thermal energy. Conversely, the circulation is stopped in order to prevent the cooling of the ground. In this way, the plant injects thermal energy only during the day. In winter season, the circulation of the system is reversed and the "Discharge Phase" occurs. More details about the Grugliasco BTES plant and the first long term results obtained since the startup of the plant can be found in Giordano et al. (2016a).

2.2 Electrical resistivity imaging

Owing to the limited dimensions of the area around the BHE field and in the need of trade-off between spatial resolution and satisfactory depth of investigation (DOI), resistivity

measurements were performed along a 72 electrode profile with inter-electrode spacing of 1 m (**Fig. 2**). Time-lapse measurements reported in this paper were carried out hourly on 2014 July 25th, from 9 AM to 4 PM. In **Tab. 1** a schedule of the executed ERT surveys is reported together with instantaneous values of flow rate, fluid temperature difference between in and out, power and energy transferred to the ground every 0.5 h. The heating activity lasted since 8-9 AM until 3-4 PM and a little cooling occurred when the collectors were no longer able to collect enough thermal energy. A Wenner-Schlumberger measuring sequence was used for acquisitions with Syscal R1 georesistivimeter (Iris Instruments). A short current injection time (250 ms) was adopted in order to record the set of measurements (total of 548 quadrupoles for each survey) as quick as possible. This configuration allowed us to obtain a reliable DOI of about 12-13 m b.g.l. in a vertical cross section. With the aim of comparing results obtainable with different computational efforts, both apparent and inverted resistivity data achieved from the surveys are hereby discussed. Since Giordano et al. (2016b) demonstrated the ability of time-lapse apparent resistivity to reach valuable temperature estimation in porous media at lab scale, thus an analogous approach was tested at the field scale.

The finite-element algorithm R2 (Version 2.7b, A. Binley, Lancaster University) was adopted to carry out the resistivity data inversion (Binley and Kemna, 2005). The inverse problem is formulated through a set of model parameters **m** (i.e. model cells resistivities), related to a set of measured data, **d**, through the relation **d**=F(**m**), F being the forward operator. The inversion algorithm is based on a least square formulation, as it minimizes the data misfit according to **Eq. [1]**:

$$\boldsymbol{\Psi}_d = \sum_{i=1}^{D} \left(\frac{F_i(\mathbf{m}) - \mathbf{d}_i}{\varepsilon_i} \right)^2 = \|\mathbf{W}_d(F_i(\mathbf{m}) - \mathbf{d}_i)\|^2 \qquad [1]$$

where D is the total number of measured data, $\mathbf{d}_i$ is the i-th observed data vector, $F_i(\mathbf{m})$ is the i-th datum obtained through the forward model solution and ε_i the variance of the i-th datum, from which the data weighing matrix $\mathbf{W}_d$ is derived (LaBrecque et al., 1996a). The inversion requires a regularization term to be minimized, in order to create a reliable and realistic result. Regularization of the model can incorporate a-priori information on the geology of the area, introducing penalties for departure from an initial model and for anisotropy in the reconstruction (**Eq. [2]**):

$$\boldsymbol{\Psi}_m = \alpha_s \|\mathbf{W}_s(\mathbf{m} - \mathbf{m}_0)\|^2 + \alpha_x \|\mathbf{W}_x(\mathbf{m} - \mathbf{m}_0)\|^2 + \alpha_z \|\mathbf{W}_z(\mathbf{m} - \mathbf{m}_0)\|^2 \qquad [2]$$

where, on the right hand side, the first term is the penalty for the deviation from a starting model $\mathbf{m}_0$, the second and third terms are penalties for roughness in horizontal and vertical direction, the $\alpha_{s,x,z}$ are the related smoothing factors and $\mathbf{W}_{s,x,z}$ are the weighting matrices composing the model regularization matrix $\mathbf{W}_m$. The total objective function $\Psi=\Psi_d+\Psi_m$ must be minimized iteratively, by searching the model improvement $\Delta\mathbf{m}_k$ that drives the model to the best-fitting solution (**Eq. [3]**):

$$\left(\mathbf{J}_k^T\mathbf{W}_d^T\mathbf{W}_d\mathbf{J}_k + \alpha\mathbf{W}_m^T\mathbf{W}_m\right)\Delta\mathbf{m}_k = \mathbf{J}_k^T\mathbf{W}_d^T\mathbf{W}_d[\mathbf{d} - \mathrm{F}(\mathbf{m}_k)] - \alpha\mathbf{W}_m^T\mathbf{W}_m(\mathbf{m}_k - \mathbf{m}_0) \quad [3]$$

where $\mathbf{J}$ is the Jacobian or "sensitivity" matrix, $\mathbf{m}_{k+1}=\mathbf{m}_k+\Delta\mathbf{m}_k$ is the updated model at k-th iteration. R2 has the possibility to build different types of finite element meshes with regular quadrilateral, general quadrilateral or triangular cells. A quadrilateral cell array was used in this case, with finite element sizes progressively increasing with increasing distance from the electrodes (i.e. with depth). The data error estimation, necessary to set the matrix $\mathbf{W}_d$, is computed according to LaBrecque et al. (1996a). The model regularization can be forced to penalize undesired departures from an *a priori* model, or to follow vertical/horizontal anisotropic reconstruction. For the present study, an isotropic regularization was maintained.

The starting model of the time-lapse inversion of the subsequent time steps was the model resulting from the inversion of background data which is the one collected at 9 AM (zero condition). Time-lapse data were inverted with the difference inversion algorithm described by LaBrecque and Yang (2001). Difference inversion is an extension of the traditional Occam's inversion and is based on the minimization of **Eq. [4]**:

$$\Delta\mathbf{d} = (\mathbf{d} - \mathbf{d}_0) - [\mathrm{F}(\mathbf{m}) - \mathrm{F}(\mathbf{m}_0)] \quad [4]$$

where $\mathbf{d}$ and $\mathrm{F}(\mathbf{m})$ represent the data vector and the forward response for the model $\mathbf{m}$ respectively, and the subscript index "0" denotes the background dataset and related forward response. The vector parameter $\mathbf{m}_0$ comes from a single inversion of the background dataset and constitutes the starting and the reference model for the difference inversion process. The model update $\Delta\mathbf{m}=\mathbf{m}_{k+1}-\mathbf{m}_k$ is obtained by solving **Eq. [5]** as an optimization problem, usually with a conjugate-gradient approach,

$$\left(\mathbf{J}_k^T\mathbf{W}_d^T\mathbf{W}_d\mathbf{J}_k + \alpha\mathbf{R}\right)\Delta\mathbf{m}_k = \mathbf{J}_k^T\mathbf{W}_d^T\mathbf{W}_d\Delta\mathbf{d} - \alpha\mathbf{R}(\mathbf{m}_k - \mathbf{m}_0) \quad [5]$$

The regularization matrix, $\mathbf{R}$, is hereby expressed as **Eq. [6]**:

$$\mathbf{R} = \left(\mathbf{J}_k^T \mathbf{W}_d^T \mathbf{W}_d \mathbf{J}_k + \alpha \mathbf{W}_m^T \mathbf{W}_m\right)^{-1} \mathbf{J}_k^T \mathbf{W}_d^T \mathbf{W}_d \mathbf{J}_k \quad [6]$$

LaBrecque and Yang (2001) proved that this algorithm is less sensitive to systematic errors in the data, more efficient in terms of computational requirements and more robust in imaging the real changes in the resistivity distribution. In fact, the method is based on the calculation of a single Jacobian matrix, which is supposed to adequately describe the sensitivity distribution of both the model at time t and the background model. This assumption implies non dramatic changes in the resistivity distribution and the process is oriented to find small perturbation with respect to the initial model.

2.3 Data error analysis

Globally, raw data showed good quality and repeatability. Apparent resistivity values ranged between 50 and 250 Ωm. Since repeatability of the measurements was available and the measured data distribution was not scattered, the 2% of the measured resistance values was taken as a reasonable weighting parameter for inverting the background dataset. In order to perform the time-lapse inversions, data errors were reduced to 1% for the subsequent datasets. With 2% error the starting model coincided with the solution and the inversion process was indeed not able to find the variations between the consecutive time steps. Few outliers, such as measurement errors and anomalous high and low apparent resistivity values, were filtered out before the inversion process, giving a dataset of 540 resistance values to be inverted.

Demonstrating the difficulty of operating in highly urbanized areas, it has been noticed that the concrete entry way to the building gets overheated around noon. Moreover, the presence of underground water pipes and electric cables supplying the nearby building were also causes of disturbance in data acquisition. This created anomalous measurements (both low and high resistance values) which behaved differently with respect to the surrounding soil. In order to get rid of noisy data, the measurements involving electrodes that fall around the entry way itself (electrodes from 33 to 38) were filtered out. Then, a reduced time-lapse dataset (with 341 quadrupoles) was also inverted. In any case, the algorithm used for resistivity inversion at Grugliasco BTES site was ideal since the data errors were likely to follow a Gaussian distribution and the resistivity model was expected to change in a smooth manner.

2.4 Temperature estimation based on resistivity values

A quantitative interpretation of resistivity data in terms of temperature variation was performed by using both apparent data and inversion results. Both data were processed according to **Eq. [7]**:

$$T_t = \frac{1}{m}\left(\frac{100}{\Delta\rho(\%)+100} - 1\right) + T_0 \qquad [7]$$

where Δρ (%) is the resistivity variation between a defined step and the zero condition, T_0 and T_t are temperatures at respective time steps and *m* is the fractional change in electrical resistivity (°C^{-1}). A range of 0.018 ÷ 0.025 °C^{-1} has been found by several authors for *m* (Revil et al., 1998; Hayashi, 2004; Hayley et al., 2007; Hermans et al., 2012) and it varies according to the type of fluid and sediments. For the present case, **Eq. [7]** was adopted with Δρ (%) obtained both from apparent and inverted resistivity. An *m* value of 0.021 °C^{-1} was assumed after calibration tests at lab scale (Giordano et al., 2016b). Reference temperature (T_0) could not be adopted homogenous within the whole investigated ground. Indeed, at the beginning of the day the BHE field showed temperature values higher than the undisturbed ground, since the charge phase started 4 months earlier. The reference temperature field was thus obtained from the values registered by temperature sensors in the boreholes and in the monitoring hole at the beginning of the day of measurements. A value of 14.2 °C was used for the undisturbed ground aside the BHE field. Then a smooth gradient was applied from the borders of the BHE field to the center of the heated volume where a temperature of 17.5 °C was registered by the sensors.

3. RESULTS

The aim of evaluating the thermally affected zone of the underground from electrical resistivity measurements is not an easy task in the test site under consideration. Firstly, the system is operating in the partially-saturated zone, so that possible complex resistivity variations can be highlighted with increasing temperature (e.g. de-saturation); secondly, the available space for the surveys is limited; lastly, the presence of several anthropic elements (entry ways, water pipes, electric cables and foundations of the buildings) could affect data collection, processing and interpretation. These are the main reasons why both apparent resistivity and true resistivity models were processed in order to highlight qualities and flaws of each one.

3.1 Apparent resistivity data

Time-lapse variations (in % with respect to the zero condition at 9 AM) of apparent resistivity for steps at 1, 2 and 3 PM are shown in **Fig. 3**. As previously mentioned, the entry way and its underlying pipes create a noticeable disturbance to the dataset (vertical anomaly at an abscissa of about 35 m). This anomaly is a combination of errors due to water pipes and electric cables (constant) and to the heat up of the entry way (variable). Constant sources of noise could be easily erased from data, while variable sources are more complicated to tackle. The portions of the ground on both sides of the concrete way are subjected to a heat up more pronounced than the other parts of the section. Besides these effects though, the BTES influence is evident between 20 and 30 m, where the decrease in resistivity is higher (-1 ÷ -2% at 3 PM) than on the right of the entry way.

Percentage differences among the resistivity pseudo-sections were processed for temperature estimation using **Eq. [7]**. Data obtained are reported in **Fig. 4** for the zone around the BHEs (for location see **Fig. 3**). The dataset population is small but the variogram spatial analysis confirmed that a valuable Kriging interpolation could be achieved. At 1 PM, a heating plume is clear around the BHEs, with temperature 2 ÷ 3 °C higher than the surrounding soil. In the successive steps, the TAZ is progressively more evident with maximum values of 18.5 °C in the core at 2 and 3 PM. An increase in temperature can also be observed at greater depths. The heated volume is symmetric at 1 PM, whereas the influence of the concrete entry way is clear in the following sections, extending the TAZ towards West.

3.2 Inverted resistivity data

The inverted background resistivity model (9 AM) for the whole dataset is shown in **Fig. 5a**. The resistivity section reports a shallow low resistivity anomaly in correspondence to the boreholes and to the excavation made up to a depth of 1.5 m to provide an insulation to the pipes. A more pronounced anomaly is also highlighted around an abscissa of 35 m, where the electrodes were hammered in the concrete bricks of the entry way. The remaining part of the model shows a relatively homogeneous medium characterized by unsaturated gravels and sands, apart from the high resistivity volume in the Eastern part, most likely due to the basement of the buildings. The same background model for the filtered dataset is reported in **Fig. 5b**. As in the aim of the filtering, this model does not show the marked low resistivity anomaly at 35 m, confirming the success of data filtering.

Results of time-lapse inversions for the same three example time steps of apparent resistivity data, respectively at 1, 2 and 3 PM, are reported for the whole dataset in **Fig. 6**. At

1 PM two small volumes of negative and positive resistivity variation are clear between 25 and 35 m. In the following steps, these anomalies increase of intensity and volume and at 3 PM a sharp contrast between a -10% and a +10% volume is located in the middle of the section. The negative variation can be related to the operation of the plant (temperature increase) while the small positive one is located below the position of the entry way. The whole resistivity distribution is however characterized by a general decrease of resistivity (-3 to -5%) apart from three volumes with positive variation. The increasing resistivity anomaly at 12 m appears to be related to the high resistivity anomaly located in the same position in the background model (**Fig. 5a**). The highest negative variation is located at 29 m. The entire volume has a lateral extension of about 10 m and seems to continue below the end of the section (> 10 m). Knowing the position of the plant, this can be ascribed to the effect of heat injection, but the highest intensity at 3 PM (-5.3%) is shifted by 4 m towards West with respect to the position of the central borehole DU. As above mentioned, the concrete-made entry way gets overheated and transfers the heat to the underground.

Results of time-lapse inversions for the same three example time steps are reported for the filtered dataset in **Fig. 7**. These results show a general smaller resistivity decrease, but still significant in correspondence of the BTES. The highest amount of negative resistivity variation at 3 PM (-2.7%) is located at 28 m, but in the top 1 ÷ 1.5 m. The filtering is successful in reducing the effect of the entry way, but at the same time it highlights the influence of the solar radiation on the surface, shifting the maximum decrease in resistivity towards the ground level.

For both datasets, resistivity values were processed in order to achieve an estimate of underground temperature distribution. **Figs. 8** and **9** report the temperature maps such obtained for the part of the resistivity section shown in **Figs. 6** and **7**, just close to BHE field. A percentage variation with respect to background (9 AM) was calculated at each cell of the volume and then adopted to get resistivity-derived temperature values (from **Eq. [7]**). Temperature data were then interpolated with Kriging algorithm, accounting for the analysis of spatial data variability.

The whole set of data (**Fig. 8**) presents a radial thermally affected zone around the central BHE, with maximum values of 17.5, 18.5 and 19.5 °C at 1, 2 and 3 PM respectively. The volume influenced by temperature increase is roughly symmetric, but the portion at 2.5 m right from the BHEs is warmer (16 °C at 1 PM) and this difference is amplified at 2 PM and 3

PM. It is interesting to note that at 3 PM the top 1.5 m is colder than the deeper portions: indeed, it is only influenced by solar radiation since the top of the boreholes is located 1.5 m b.g.l., with a thermal insulation above this depth.

The filtered dataset (**Fig. 9**) shows lower temperatures as expected, with 18 °C as maximum value reached at 3 PM in the center of the BHE field. Thermally affected zone is symmetric with respect to the central BHE; a shift towards the Western part is not significant but still noticeable at 3 PM. This means that the influence of the overheated concrete way is higher than expected, but filtering more data would reduce the reliability of the data inversion too much. The top of the BHEs is not visible, even in the last considered step. As explained above, after filtering the noisy data out, the maximum decrease in resistivity is shifted towards the ground level. This can be explained by considering that some of the filtered data, at the center of the BHE system and at 8 ÷ 12 m of depth, appeared significantly influenced by the entry way. The shallowest data are nevertheless equal before and after filtering, since a temperature of 18 °C is reached between the abscissa range 25.5 ÷ 27.5 m in both datasets. Therefore, the action of filtering contributed to reduce the resistivity decrease in the whole section, but it did not provide a noteworthy improvement of the TAZ imaging.

4. DISCUSSION

A detailed discussion can be conducted in order to highlight qualities and flaws of the adopted methodologies, that can serve as fast and reliable qualitatively TAZ imaging and quantitative temperature investigation tools.

Fig. 10 reports a graph with the temperature recordings of the control system in two of the four BHEs (A and DU) and in the monitoring hole (MH), and the resistivity-derived temperatures achieved by the three methods above described. Resistivity-derived temperatures are reported for points located in correspondence of DU and MH at 6 m of depth (black asterisks in **Figs. 3**, **6** and **7**), while temperature values from the monitoring system are obtained by averaging along the entire drilling depth the values of temperature sensors (4 Pt-100 sensors, every 5 m).

At a first glance, it can be noticed that the direct temperature data are not perfectly in agreement with resistivity-derived temperatures. Owing to the operative mode of the plant, the highest temperatures are observed in the DU, reaching a peak between 1 and 3 PM at around 23 °C, while the outer borehole A shows reduced temperatures. Resistivity-derived

temperatures appear roughly comparable to the data from the outer BHEs ranging between 18.5 and 19.5 °C, but with an apparently delayed peak. It is important to note that temperature sensors in the boreholes (DU and A), owing to operational issues, are attached to plastic pipes where the HTF flows (temperatures of about 30 ÷ 33 °C in DU and 24 ÷ 25 °C in A have been monitored throughout the day). This obviously can result in higher values with respect to the real ground temperatures, which are supposed to be better imaged by resistivity data.

Data from the monitoring hole are instead not affected by the presence of the HTF. These data are almost stable throughout the day. In the long term, MH data show indeed an increasing temperature trend of about 0.5 °C/month which is a too low gradient to show a significant daily variation. However, resistivity-derived temperatures in a location proximal to the MH describe a trend more similar in time and smaller in temperature increase to data near the BHEs. This can be explained by the influence of the BHEs to the whole resistivity distribution, which coarse resolution struggles to differentiate and to image a distinct situation between DU and MH. We can estimate that temperature amounts to 20 ÷ 21 °C at 2 ÷ 3 PM in the core and to around 16 °C at the limit of a 2-m-radius circle. This temperature difference (4 ÷ 5 °C) should be highlighted by a -10 % resistivity variation that in fact is smoothed within the ground volume where the boreholes are placed.

Temperature estimation derived by inverted resistivity values on the whole dataset outputs the highest temperatures both in DU and MH, as already described in the previous section. Inverted resistivities on the filtered dataset allowed us to reduce the contribution of the overheating on the entry way and to decrease the temperature trend at the same time. Temperature peaks are therefore 1 ÷ 1.2 °C lower at both monitoring points at 3 PM. Values achieved by processing only apparent resistivities are a valid compromise between the previous processing approaches. The direct imaging of apparent resistivity data could therefore be considered as a valuable approach for the qualitative imaging of the TAZ and a rough estimation of the temperature increase. This could moreover be obtained with significantly less computational effort in data elaboration and could be potentially used as an indirect monitoring tool.

The imaged TAZ by all the data presented appears to be reliable, considering the reduced dimensions and energy input (**Tab. 1**) of the living lab and the unsaturated material characterizing the subsoil. Available literature data of similar setup in the vadose zone are scarce. Moradi et al. (2016) presented an interesting experimental lab scale setup where a

BTES was simulated in an unsaturated porous medium and heat transfer mechanisms were tested and numerically analyzed. The area outside the BHE field reached 10 to 15 °C increase after each experiment lasting 8 h, but the finite dimensions of the apparatus and the absence of the geothermal grout around the plastic pipes make it difficult to do a thorough comparison with our field-scale living lab. An easier comparison can be done with the work by Rapantova et al. (2016); a BTES fed by a CHP plant injects in the charge phase (6 months) around 500-600 GJ in a geological section made of water-saturated gravels and sands (about 10 m) overlying a claystone formation. The numerical results showed that in the alluvial deposits the ground temperature is no more disturbed by heat injection at around 6 m from the outermost BHE at the end of the injection phase. In the underlying claystones, where conduction is the predominant heat transfer mechanism and it can be roughly comparable to the present study, at 4.5 m no disturbance is registered. Considering that the Grugliasco plant injected around 1.5% of that amount of energy in 6 months (9 GJ from Giordano et al., 2016a), the thermal plume extension and intensity highlighted by the ERT monitoring in the present work is consistent with the energy input and the geological setting.

To sum up, a qualitative TAZ imaging of the plant was successfully achieved, but the same is not true with respect to the quantitative estimation. This can also be partially related to the lack of precise independent temperature recordings from the monitoring system for a valuable comparison (i.e. not affected by the presence of the HTF). However, MH values report that all the three resistivity-derived temperature trends tend to overestimate the real ground thermal behavior at 2 m from the central BHE. This can be mainly related to a non-optimal resolution of the acquisition, to the intrinsic smoothing of the resistivity method and to the already discussed disturbances that create significant noise in the datasets.

5. CONCLUSIONS

Time-lapse resistivity surveys carried out on a BTES living lab in Grugliasco (Torino, Italy) in order to image the thermally affected zone have been reported. Measurements were performed hourly from 9 AM to 4 PM with a linear 72-electrode 1-m spaced array and both apparent and true resistivity values were adopted as a qualitative and quantitative TAZ imaging tool. Different types of data processing were adopted in order to face issues mainly related to a highly man-made environment.

Thanks to the direct monitoring system set up on the BTES living lab, temperature recordings in three BHEs and in the MH allowed us to define the initial temperature (T_0) and

thus to achieve a valuable qualitative TAZ imaging. Nevertheless, the temperature prediction from resistivity variation acquired throughout the day was not completely reliable if compared with direct recordings. It is however true that standalone sensors chains are not available in the BTES core and those adopted for comparison were strongly affected by HTF flowing within the plastic pipes. Results from all the three adopted methodologies showed a rather homogeneous temperature distribution from the center up to a 2 m distance (MH position), with difficulties in detecting temperature differences within a couple of meters. This can be partially attributed to the intrinsic spatial smoothing of the ERT method itself.

Apparent resistivity differences proved to be in valid agreement with inverted results, behaving as an average between the entire dataset and the filtered dataset. In fact, the inversion process did not allow us to significantly improve qualitative and quantitative TAZ imaging in comparison to the pseudo-sections, even removing part of the data located beneath and around the entry way. This suggests the usefulness of even apparent resistivity data alone for a rough monitoring of TAZ in this kind of applications.

Future research will focus on surface 3D electric surveys and cross-borehole tomographies around the BHE site in order to improve resolution and DOI of the resistivity acquisitions. A 3D numerical simulation will moreover be carried out to serve as consistent background thermal model to perform a reliable comparison with resistivity-derived temperatures.

ACKNOWLEDGEMENTS

The GTES Living Lab in Grugliasco was mainly funded by 2 local project by *Alcotra Innovazione* in 2012 and *P.O.R.-F.E.S.R.* in 2013.

The authors would moreover like to thank the anonymous reviewers for the useful comments and advices that improved the structure of the paper.

REFERENCES

Arato, A., Boaga, J., Comina, C., De Seta, M., Di Sipio, E., Galgaro, A., Giordano, N., Mandrone, G., 2015. Geophysical monitoring for shallow geothermal applications – two Italian case histories. First Break – Near Surface Geoscience **33(8)**: 75-79.

Archie, G.E., 1942. The electrical resistivity log as an aid in determining some reservoir characteristics. Transactions of the American Institute of Mining, Metallurgical and Petroleum Engineers, **146(1)**: 54-62.

Bakema, G., Snijders, A.L., Nordell, B., 1995. Underground Thermal Energy Storage, State of the Art Report 1994. Arnhem, The Netherlands, 83 pp.

Benderitter, Y., Tabbagh, J., 1982. Heat storage in a shallow confined aquifer: Geophysical tests to detect the resulting anomaly and its evolution with time. Journal of Hydrology, **56**: 85-98.

Binley, A., Winship, P., West, L.J., Pokar, M., Middleton, R., 2002. Seasonal variation of moisture content in unsaturated sandstone inferred from borehole radar and resistivity profiles. Journal of Hydrology, **267(3-4)**: 160-172.

Binley, A., Kemna, A., 2005. Electrical Methods. In: Hydrogeophysics by Rubin and Hubbard (Eds.), 129-156, Springer

Bruno, P.P.G., Paoletti, V., Grimaldi, M., Rapolla, A., 2000. Geophysical exploration for geothermal low enthalpy resources in Lipari Island, Italy. Journal of Volcanology and Geothermal Research, **98**: 173-188.

Cabeza, L.F., 2015. Advances in thermal energy storage systems – methods and applications. Woodhead Publishing Series in Energy, Cambridge, UK, 592 pp.

Carrier, W.D., 2003. Goodbye, Hazen; Hello, Kozeny-Carman. Technical note in Journal of Geotechnical and Geoenvironmental Engineering, **129(11)**: 1054-1056.

Casasso, A., Sethi, R., 2014. Efficiency of closed loop geothermal heat pumps: A sensitivity analysis. Renewable Energy, **62**: 737-746.

Corwin, C.L., Lesch, S.M., 2005. Characterising soil spatial variability with apparent soil electrical conductivity – I. Survey protocols. Computers and Electronics in Agriculture, **46**: 103-133.

Daily, W., Ramirez, A., 1992. Electrical resistivity tomography of vadose water movement. Water Resources Research, **28(5)**: 1429-1442.

Firmbach, L., Schelenz, S., Vienken, T., Kolditz, O., Dietrich, P., 2013. Geoelectric measurements as an efficient monitoring strategy for shallow geothermic reservoirs. 2nd International Workshop on Geoelectrical Monitoring, Berichte Geol. B.-A., 104.

Fisch, M.N., Guigas, M., Dalenbäck, J.O., 1998. A review of large-scale solar heating systems in Europe. Solar Energy **63(6)**: 355-366.

Fragkogiannis, G., Papatheodorou, N., Stamataki, S., 2008. Evaluation of Thermal Performance of Ground - Source Energy Systems. A geophysics supported approach. World Renewable Energy Congress X and Exhibition, July 19th-25th, Glasgow, Scotland.

Friedman, S.P., 2005. Soil properties influencing apparent electrical conductivity: a review. Computers and Electronics in Agriculture, **46**: 45-70.

Garg, S.K., Pritchett, J.W., Wannamaker, P.E., Combs, J., 2007. Characterization of geothermal reservoirs with electrical surveys: Beowave geothermal field. Geothermics, **36**: 487-517.

Giordano, N., Comina, C., Mandrone, G., Cagni, A., 2016a. Borehole thermal energy storage (BTES). First results from the injection phase of a living lab in Torino (NW Italy). Renewable Energy, **86**: 993-1008, doi: 10.1016/j.renene.2015.08.052.

Giordano, N., Comina, C., Mandrone, G., 2016b. Laboratory scale geophysical measurements aimed at monitoring the thermal affected zone in Underground Thermal Energy Storage (UTES) applications. Geothermics, **61**: 121-134, doi: 10.1016/j.geothermics.2016.01.011.

Hayashi, M., 2004. Temperature-electrical conductivity relation of water for environmental monitoring and geophysical data inversion. Environmental Monitoring and Assessment, **96**: 119-128, doi: 10.1023/B:EMAS.0000031719.83065.68.

Hayley, K., Bentley, L.R., Gharibi, M., Nightingale. M., 2007. Low temperature dependence of electrical resistivity: Implications for near surface geophysical monitoring. Geophysical Research Letters, **34**: L18402, doi: 10.1029/2007GL031124.

Hermans, T., Vandenbohede, A., Lebbe, L., Nguyen, F., 2012. A shallow geothermal experiment in a sandy aquifer monitored using electric resistivity tomography. Geophysics, **77(1)**: B11-B21.

Hermans, T., Wildemeersch, S., Jamin, P., Orban, P., Brouyère, S., Dassargues, A., Nguyen, F., 2015. Quantitative temperature monitoring of a heat tracing experiment using cross-borehole ERT. Geothermics, **53**: 14-26.

Hoffmann, R., Dietrich, P., 2004. Geoelectrical measurements for the determination of groundwater flow directions and velocities. Grundwasser, **9(3)**: 194-203.

LaBrecque, D. J., Miletto, M., Daily, W., Ramirez, A., Owen, E., 1996a. The effect of noise on Occam's inversion of resistivity tomography data. Geophysics, **61**: 538–548.

LaBrecque, D.J., Ramirez, A.L., Daily, W.D., Binley, A.M., Schima, S.A., 1996b. ERT monitoring of environmental remediation processes. Measurement Science and Technology, **7**: 375-383.

LaBrecque, D.J., Yang, X., 2001. Difference inversion of ERT data: A fast inversion method for 3-D in situ monitoring. Journal of Environmental and Engineering Geophysics, **6(2)**: 83-89.

Lüders, K, Firmbach, L., Ebert, M., Dahmke, A., Dietrich, P., Köber, R., 2016. Gas-phase formation during thermal energy storage in near-surface aquifers: experimental and modelling results. Environmental Earth Sciences, **75(21)**: 1404.

Michot, D., Benderitter, Y., Dorigny, A., Nicoullaud, B. King, D., Tabbagh, A., 2003. Spatial and temporal monitoring of soil water content with an irrigated corn crop cover using surface electrical resistivity tomography. Water Resources Research, **39(5)**: 273-285.

Miller, C.R., Routh, P.S., Brosten, T.R., McNamara, J.P., 2008. Application of time-lapse ERT imaging to watershed characterization. Geophysics, **73(3)**: G7-G17.

Moradi, A., Smits, K.M., Lu, N., McCartney, J.S., 2016. Heat transfer in unsaturated soil with application to borehole thermal energy storage. Vadose Zone Journal, **15(10)**, doi: 10.2136/vzj2016.03.0027.

Nguyen, A., Pasquier, P., Marcotte, D., 2017. Borehole thermal energy storage systems under the influence of groundwater flow and time-varying surface temperature. Geothermics, **66**: 110-118.

Ramirez, A., Daily, W., LaBrecque, D., Owen, E., Chesnut, D., 1993. Monitoring an underground steam injection process using electrical resistance tomography. Water Resources Research, **29(1)**: 73-87.

Rapantova, N., Pospisil, P., Koziorek, J., Vojcinak, P., Grycz, D., Rozehnal, Z., 2016. Optimisation of experimental operation of borehole thermal energy storage. Applied Energy, **181**: 464-476.

Rein, A., Hoffman, R., Dietrich, P., 2004. Influence of natural time-dependent variations of electrical conductivity on DC resistivity measurements. Journal of Hydrology, **285**: 215-232.

Reuss, M., Beuth, W., Schmidt, M., Schoelkopf, W., 2006. Solar district heating with seasonal storage in Attenkirchen. ECOSTOCK 2006, in: 10th International Conference on Thermal Energy Storage, Stockton, USA.

Revil, A., Cathles, L.M., Losh, S., Nunn, J.A., 1998. Electrical conductivity in shaly sands with geophysical applications. Journal of Geophysical Research, **103**: 23925-23936, doi: 10.1029/98JB02125.

Revil, A., Karaoulis, M., Srivastava, S., Byrdina, S., 2013. Thermoelectric self-potential and resistivity data to localize the burning front of underground coal fires. Geophysics, **78**: B259–B273.

Robert, T., Hermans, T., Dumont, G., Nguyen, F., Rwabuhungu, D.E., 2013. Reliability of ERT-derived temperature – Insights from laboratory measurements. Near Surface Geoscience, Proceedings of 19th European Meeting of Environmental and Engineering Geophysics, TuS2a10, Bochum, Germany, 9-11 September 2013.

Schwartz, B.F., Schreiber, M.E., Yan, T., 2008. Quantifying field-scale soil moisture using electrical resistivity imaging. Journal of Hydrology, **362**: 234-246.

Sharma, A., Tyagi, V.V., Chen, C.R., Buddhi, D., 2009. Review on thermal energy storage with phase change materials and applications. Renewable and Sustainable Energy Reviews, **13(2)**: 318-345.

Sibbitt, B., McClenahan, D., Djebbar, R., Thornton, J., Wong, B., Carriere, J., Kokko, J., 2012. The performance of a high solar fraction seasonal storage district heating system – five years of operation. Energy Procedia, **30**: 856-865, doi: 10.1016/j.egypro.2012.11.097.

Slater, L., Binley, A.M., Daily, W., Johnson, R., 2000. Cross-hole electrical imaging of a controlled saline tracer injection. Journal of Applied Geophysics, **44**: 85-102.

Slater, L., 2007. Near surface electrical characterization of hydraulic conductivity: from petrophysical properties to aquifer geometries – A review. Surveys in Geophysics, **28**: 169-197.

Urish, D.W., 1981. Electrical resistivity-hydraulic conductivity relationships in glacial noutwash aquifers. Water Resources Research, **17(5)**: 1401-1408.

Wang, H., Qi, C., Du, H., Gu, J., 2009. Thermal performance of borehole heat exchanger under groundwater flow: A case study from Baoding. Energy and Buildings, **41(12)**: 1368-1373.

Xu, J., Wang, R.Z., Li, Y., 2014. A review of available technologies for seasonal thermal energy storage. Solar Energy, **103**: 610-638.

Zhou, Q.Y., Shimada, J., Akira, S., 2001. Three-dimensional spatial and temporal monitoring of soil water content using electrical resistivity tomography. Water Resources Research, **37(2)**: 273-285.

Figure Captions

Fig. 1 a) Schematic geological cross-section at the field test site. b) Cross-section of the BTES plant: the monitoring hole is a piezometer that serves as water table check in case of rise.

Fig. 2 Plan view of the Grugliasco BTES plant with the position of the ERT survey.

Fig. 3 Time-lapse variation (in %) of apparent resistivities at 1, 2 and 3 PM. Highlight of imaging section in Fig. 4 and temperature comparison points in Fig. 10 are also shown.

Fig. 4 Resistivity-derived temperature values achieved from the variation of apparent resistivities at 1, 2 and 3 PM.

Fig. 5 Inverted resistivity section at 9 AM, used as background for the calculation of resistivity variations: a) whole dataset; b) filtered dataset (data from electrode 33 to 38 were removed)

Fig. 6 Time-lapse variation (in %) of inverted resistivities for the whole dataset at 1, 2 and 3 PM. Highlight of section in Fig. 8 and temperature comparison points in Fig. 10 are also shown.

Fig. 7 Time-lapse variation (in %) of inverted resistivities for the filtered dataset at 1, 2 and 3 PM. Highlight of section in Fig. 9 and temperature comparison points in Fig. 10 are also shown.

Fig. 8 Resistivity-derived temperature values achieved from the variation of inverted resistivities for the whole dataset at 1, 2 and 3 PM.

Fig. 9 Resistivity-derived temperature values achieved from the variation of inverted resistivities for the filtered dataset at 1, 2 and 3 PM.

Fig. 10 Comparison between temperature data recorded by the sensors in the BTES plant (A and DU boreholes and MH) and those derived by the resistivity variation of points at specific locations (23 and 25 m on x at 6 m depth).

Tables

Tab. 1 Plant data collected during July 25th. Time of ERT surveys is also indicated.

Time	ERT surveys	Flow rate [l h^{-1}]	Tin-Tout [°C]	Power [W]	Energy [kJ]
7 AM		0	0.1	0	0
7.30 AM		0	0.1	0	0
8 AM		70	5.0	404	727.2
8.30 AM		70	7.8	636	1144.8
9 AM	survey 0	90	11.9	1246	2242.8
9.30 AM		170	7.5	1483	2669.4
10 AM	survey 1	210	10.3	2520	4536.0
10.30 AM		180	9.1	1901	3421.8
11 AM	survey 2	80	8.6	803	1445.4
11.30 AM		80	9.8	909	1636.2
12 PM	survey 3	210	13.2	3212	5781.6
12.30 PM		110	9.8	1259	2266.2
1 PM	survey 4	170	13.3	2620	4716.0
1.30 PM		210	12.5	3060	5508.0
2 PM	survey 5	100	13.2	1539	2770.2
2.30 PM		90	11.0	1149	2068.2
3 PM	survey 6	210	9.8	2391	4303.8

3.30 PM		180	7.8	1633	2939.4
4 PM	survey 7	210	11.1	2718	4892.4
4.30 PM		200	8.6	1998	3596.4
5 PM		30	6.2	217	390.6
5.30 PM		70	9.2	750	1350.0
6 PM		40	5.0	234	421.2

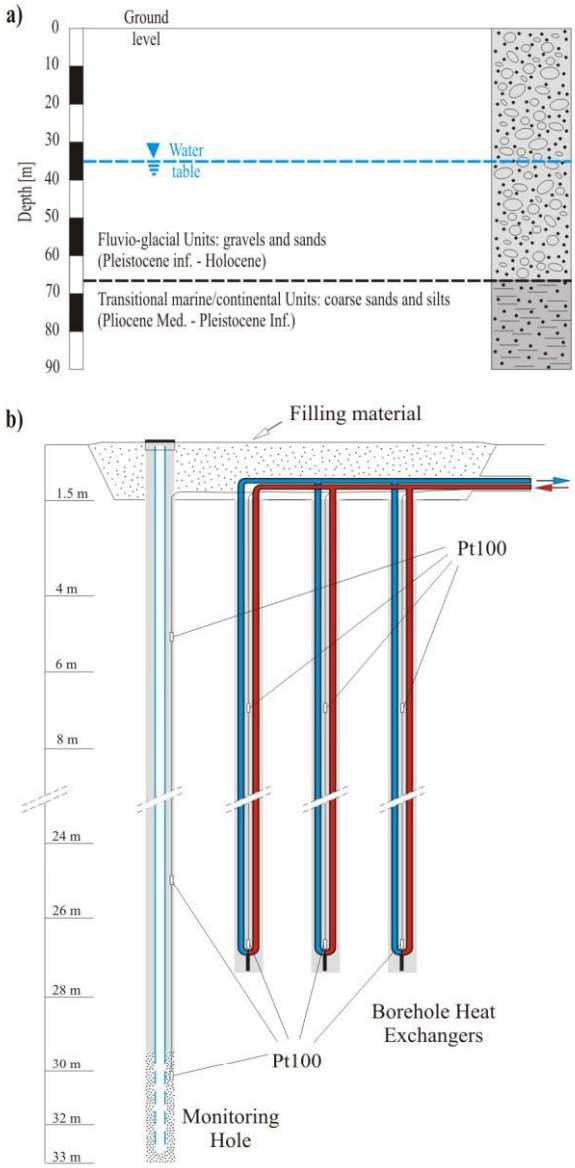

Fig. 1

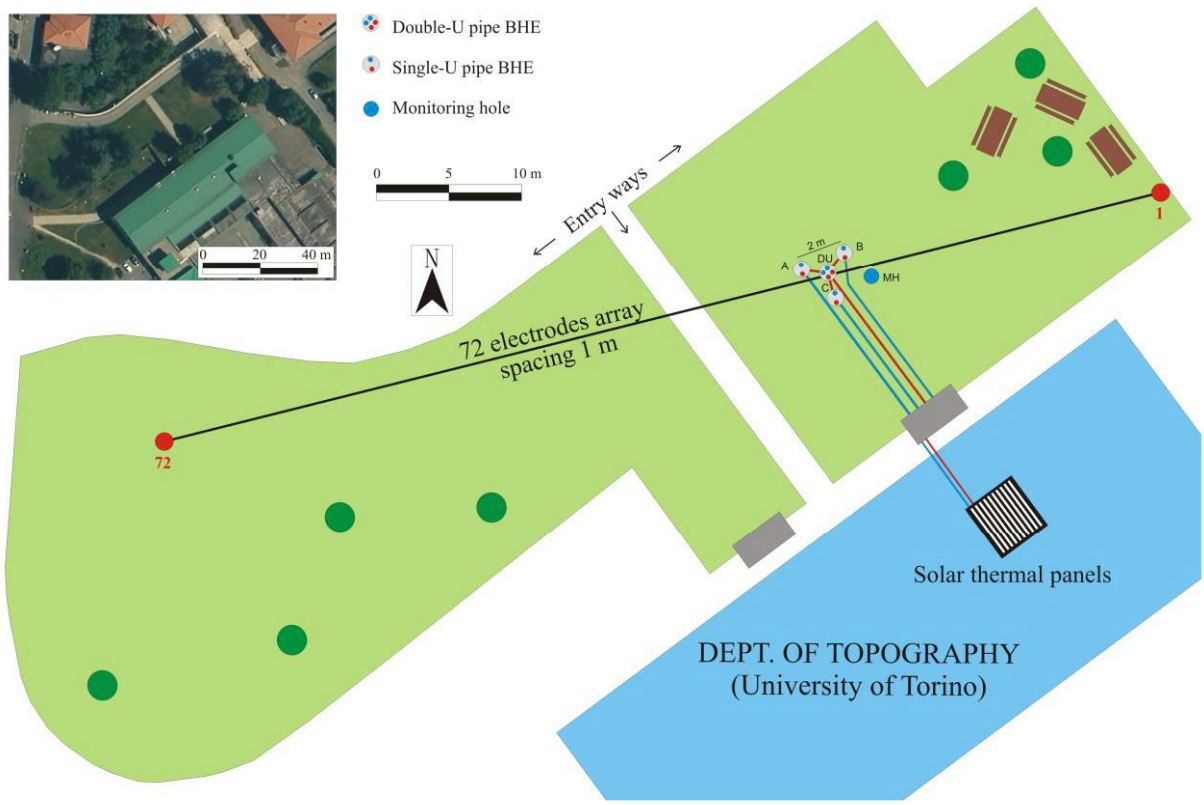

Fig. 2

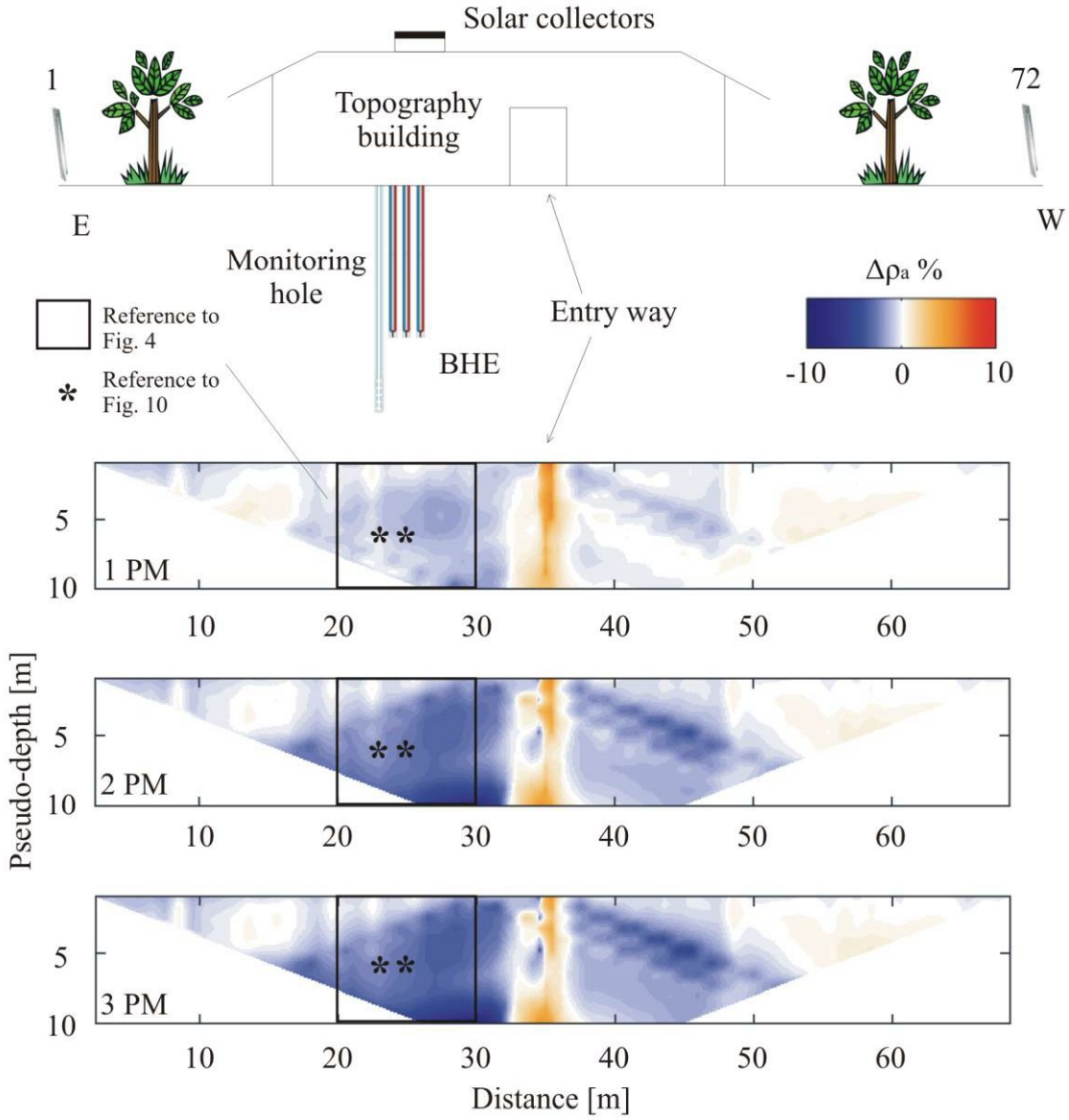

Fig. 3

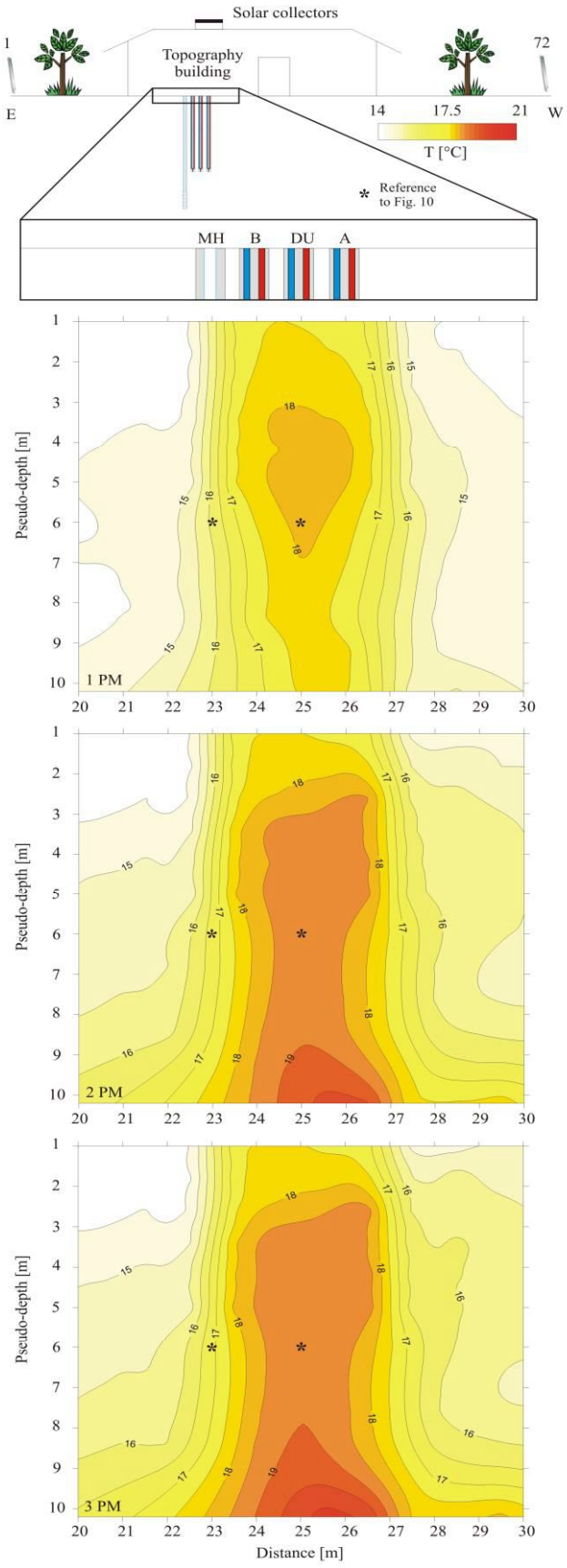

Fig. 4

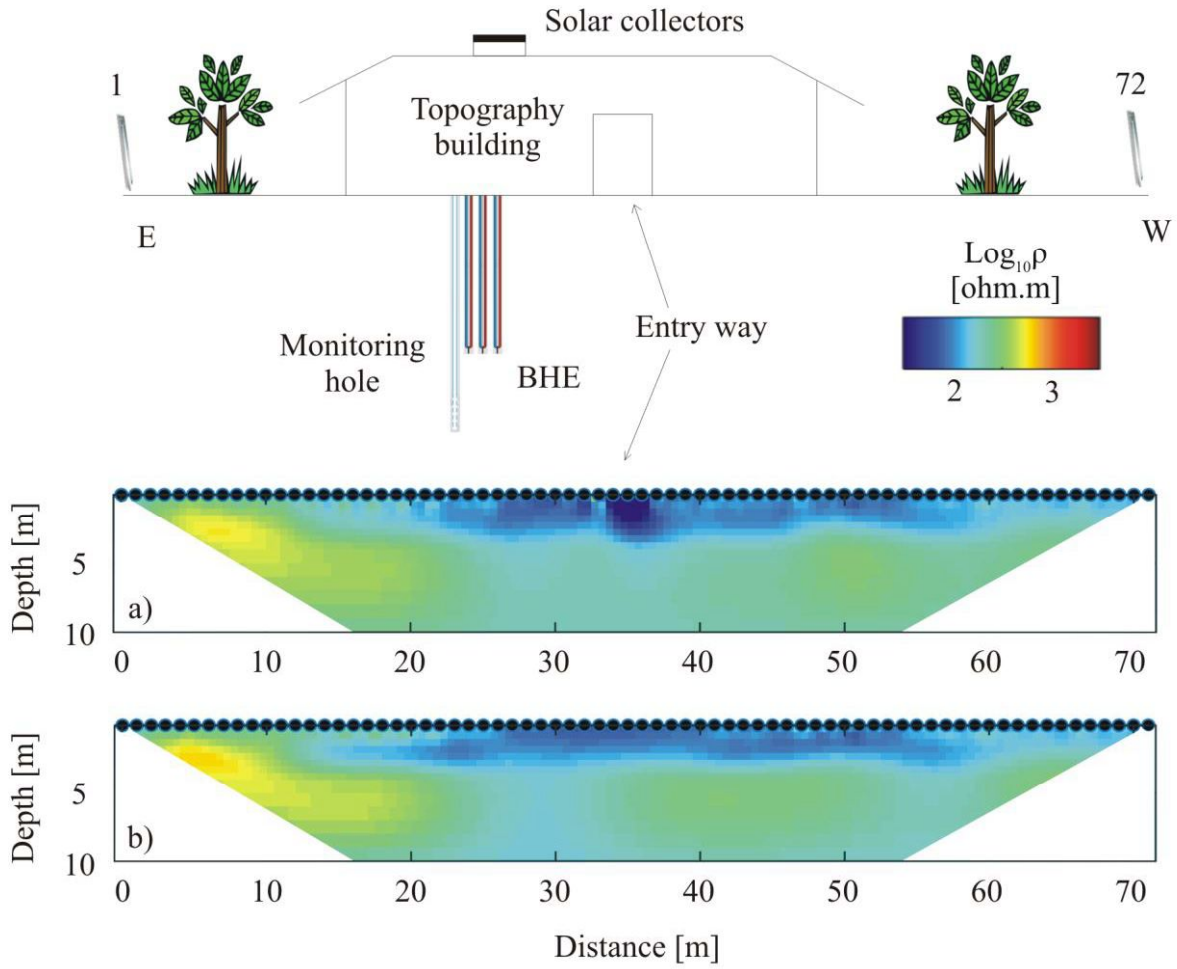

Fig. 5

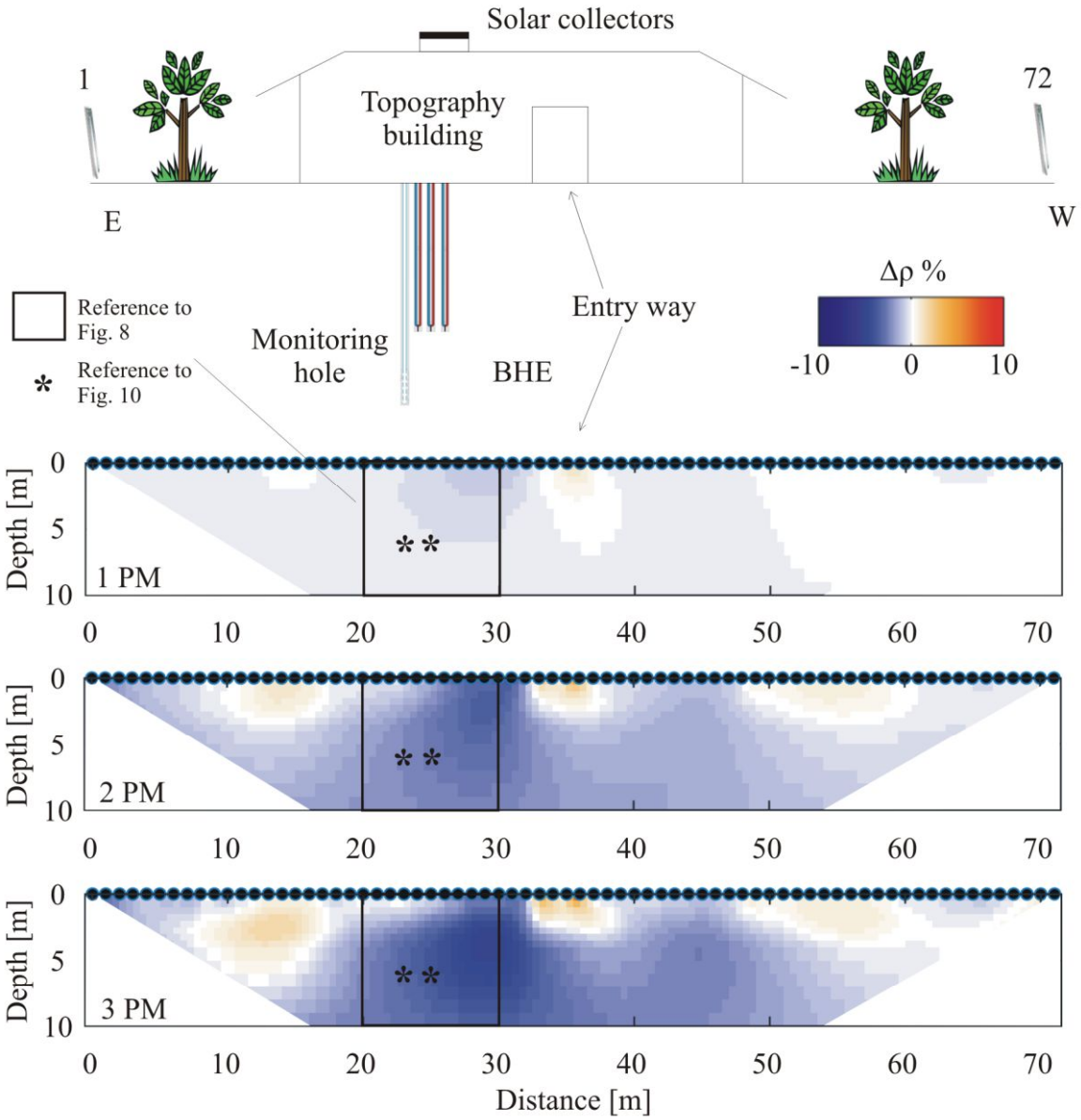

Fig. 6

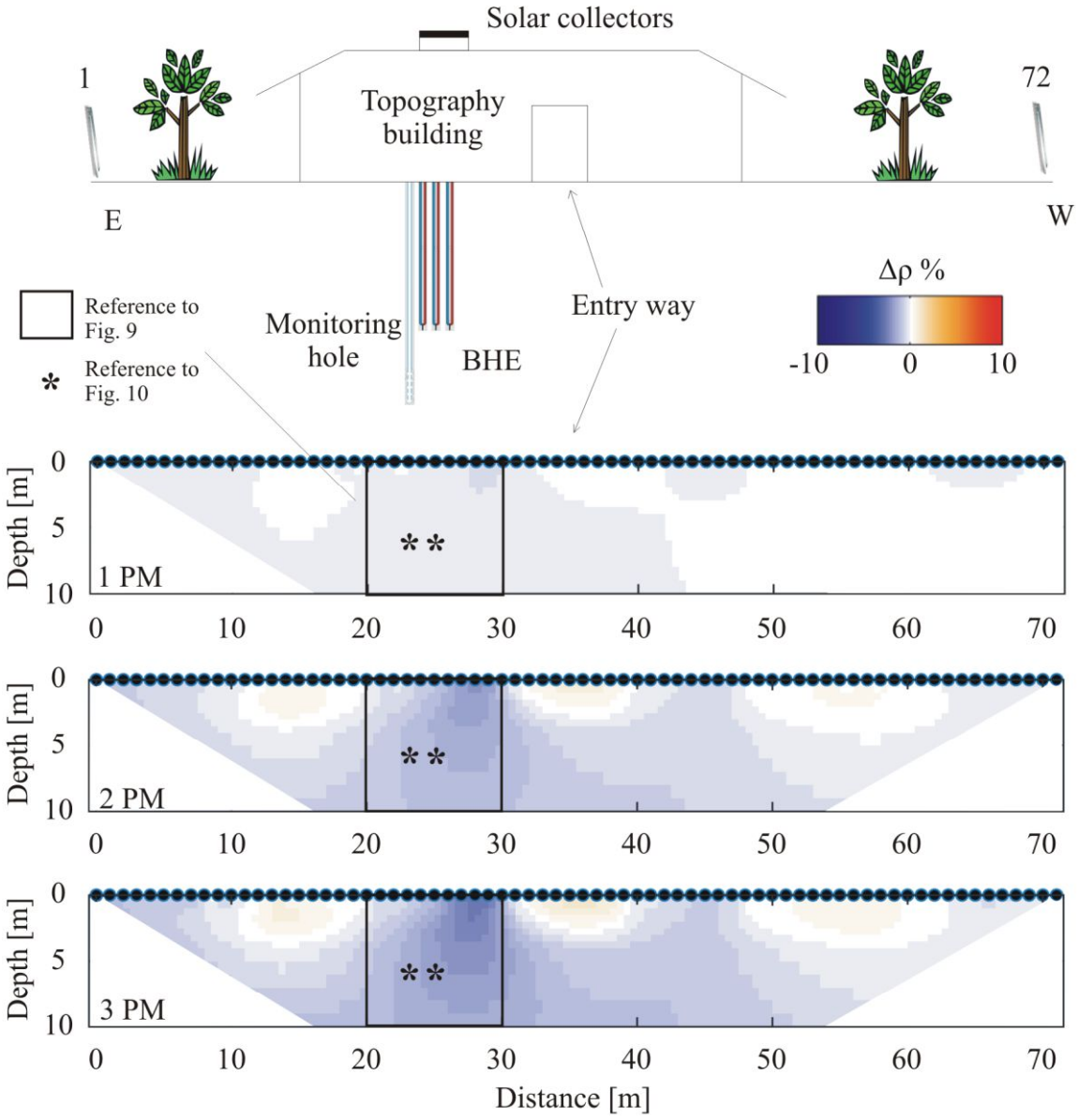

Fig. 7

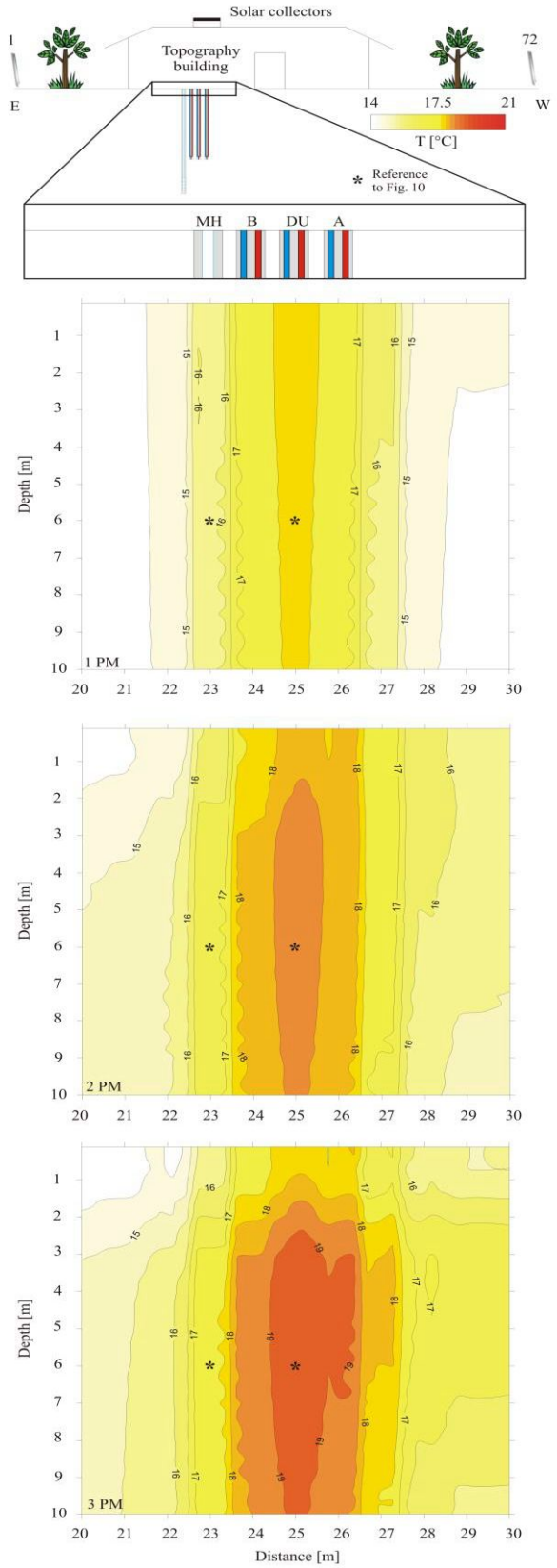

Fig. 8

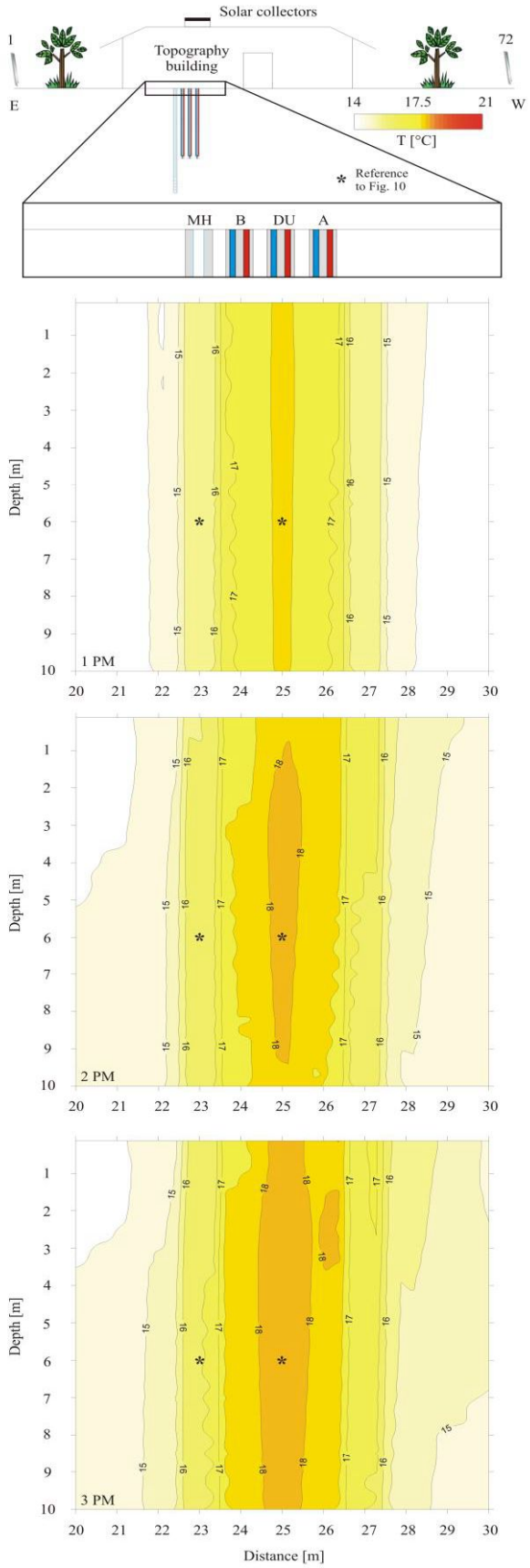

Fig. 9

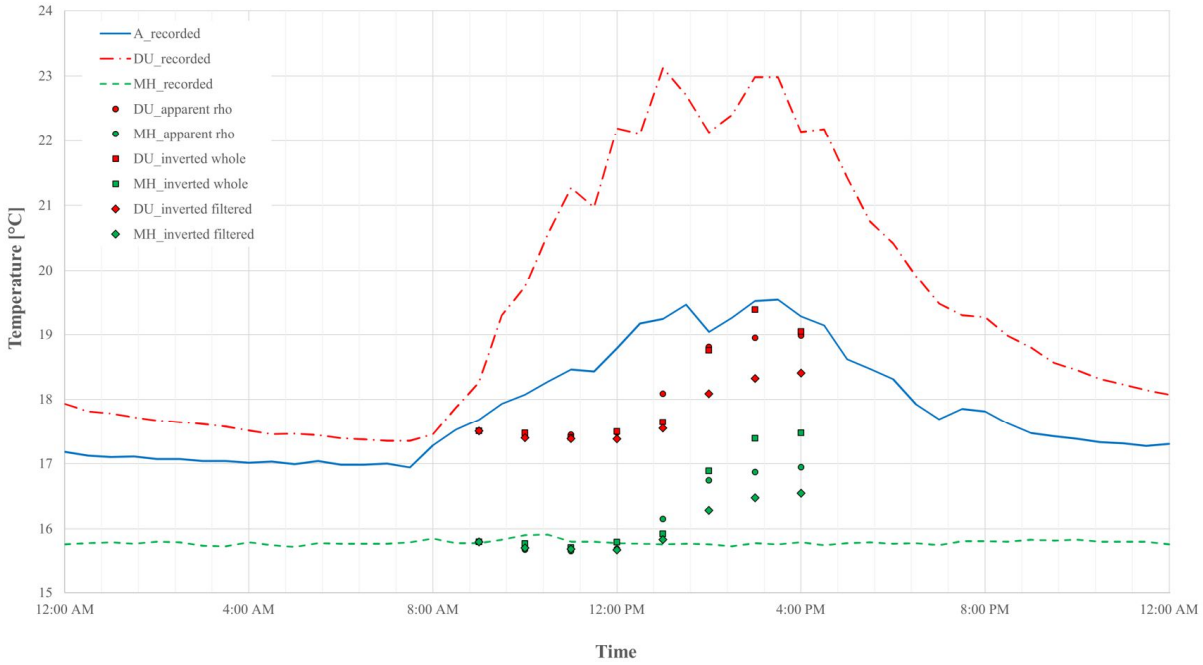

Fig. 10

Highlights

- ERT was used to image the thermally affected zone of a BTES;
- Both apparent data and inverted results were adopted;
- Resistivity-derived temperatures were compared to values from direct monitoring;
- Apparent data can provide valuable interpretation as inverted results;